Materials Research Proceedings **25** (2023) 171-178 https://doi.org/10.21741/9781644902417-22

Numerical and experimental investigations of piercing fibre-reinforced thermoplastics

Benjamin Gröger[a*], Jingjing Wang[b], René Füßel[c], Juliane Troschitz[d], Daniel Köhler[e], Christian Vogel[f], Andreas Hornig[g], Robert Kupfer[h] and Maik Gude[i]

Institute of Lightweight Engineering and Polymer Technology, Technische Universität Dresden, Holbeinstraße 3, 01307 Dresden, Germany

[a]benjamin.groeger@tu-dresden.de, [b]jingjing.wang@tu-dresden.de, [c]rene.fuessel@tu-dresden.de, [d]juliane.troschitz@tu-dresden.de, [e]daniel.koehler@tu-dresden.de, [f]christian.vogel@tu-dresden.de, [g]andreas.hornig@tu-dresden.de, [h]robert.kupfer@tu-dresden.de, [i]maik.gude@tu-dresden.de

Keywords: Joining, Simulation, Fluid-Structure Interaction

Abstract. The joining of continuous fibre-reinforced thermoplastic composites (TPC) by means of plastic deformation often results in a complex material structure in the forming zone. Especially process- and material-related parameters have high influence on the local deformation behaviour and therefore on the properties of the joint. In this paper, the focus is on mechanical joining processes based on the principle of moulding holes by a tapered pin. For the investigations, a simplified test is used in which the pin is pushed through a heated TPC plate in the thickness direction. By the pin movement the fibres and molten matrix are displaced radially and along the tool motion direction. Detailed investigations of the resultant material structure by computed tomography and numerical simulations are performed with varying pin tool geometries with bidirectional TPC material. For numerical analysis, the Arbitrary-Lagrangian-Eulerian method combined with a multi-filament approach is used. The result show that the tool geometry has a strong influence on the piercing force, the resultant material structure, and the occurring phenomena. It could be shown, that the simulation is capable to predict the resultant material structure.

Introduction

With their high specific stiffness and strength thermoplastic composites (TPC) offer a good opportunity to achieve a high degree of lightweight and increase resource efficiency. Due to the inhomogeneous inner material structure of orientated brittle fibres and ductile isotropic thermoplastic matrix an anisotropic material behaviour results. Hence, a variety of novel joining technologies have already been developed to join TPC components to adjacent assemblies. Bonding, the state of the art joining method, requires high standards for preparation and long curing times. Therefore, new mechanical joining technologies are in the scope of research [1], especially in the field of clinching technology [2]. The local forming processes of this joining method lead to a change of the material structure [3]. The changed material structure directly influences the load bearing behaviour and the capacity of the joints [4].

In thermal-assisted mechanical joining processes for metal-TPC-joints a tool [5] or auxiliary element [6] is moved in thickness direction through the material generating a hole and a form closure. Depending on process conditions (e.g. tool concept and velocity, process temperature), material properties of the matrix (e.g. melting temperature) and fibres (e.g. Young's modulus, fracture strain) different material structure phenomena occur during hole forming [7]. Due to the softening of the matrix at higher temperatures, the viscous character of the matrix increases. Consequently, the fibre-matrix interactions (FMI) can be described as a fluid-structure-interaction

Materials Research Proceedings **25** (2023) 171-178 https://doi.org/10.21741/9781644902417-22

(FSI). Besides fibre-fibre interactions (FFI) can be observed [7]. Joining by piercing based on moulded holes is characterized by a displacement of fibres in in- and out-of-plane direction caused by pin penetration [8] and independent matrix flows around the pin [9]. Such joints are often assessed by the resultant load bearing behaviour in structural tests [10]. The required joining force to displace fibres and matrix for a single pin often cannot be measured due to the test setup [11] or the application of multi-pin arrays [12]. In [8] a single pin geometry is used for joining and the influence of heating area and temperature on the joining force and resultant material structure is investigated. Due to the temperature gradients in most processes, the joining zone cannot be assumed to be isothermal. This leads to a different material behaviour within TPC because of the temperature dependency of the matrix.

By simulating such joining processes, the resultant material structure and load bearing capacity can be predicted. However, this requires the modelling of the textile architecture [13] for continuous fibres. For moulded holes with in-plane reorientation of the fibres, also an analytical approach is used in [14] to predict the fibre path.

In the present paper, the interaction of the piercing process and material structure is shown. Therefore, a simple test setup with different pin geometries is used. Due to a lack of information when using transient local heating, the whole test setup is heated up to process temperature and kept constant instead. The resultant material structure is investigated by computed tomography (CT). Based on the findings, numerical models are developed and evaluated. A multi-scale approach and the Arbitrary-Lagrangian-Eulerian (ALE)-method is used [15].

Experimental setup

The specimens are made of multi-layered uni-directional glass fibre (GF) reinforced polypropylene (PP) Borealis BJ-100HP with a melting temperature of 165 °C. The specimens are made of four unidirectional TPC-sheets with layup of $[0°/90°]_s$, and have a thickness of 2 mm with a dimension of (80 x 80) mm^2.

The test setup shown in Fig. 1a is integrated in a standard testing machine Zwick Z1465 (ZwickRoell GmbH & Co KG) equipped with a heating chamber and a 100 kN load cell. The isothermal conditions of 180 °C, controlled by three thermocouples at the specimen, the pin and within the chamber, are realized within a dwell time of 30 min. To prevent sticking between the heated specimen and the die/blank holder, thin perforated films (0.2 mm) made of polytetraflour-ethylene are fixed to the metal parts. The pin is pushed path-controlled with a velocity of 1000 mm/min into the TPC. After the piercing process, the pin rests within the TPC until the specimen temperature is cooled down to 150 °C by an air flow system near the pin. To investigate the process-structure-interaction (PSI) in terms of the tool-structure-interaction, two different pin geometries shown in Fig. 1b are used.

Materials Research Proceedings **25** (2023) 171-178 https://doi.org/10.21741/9781644902417-22

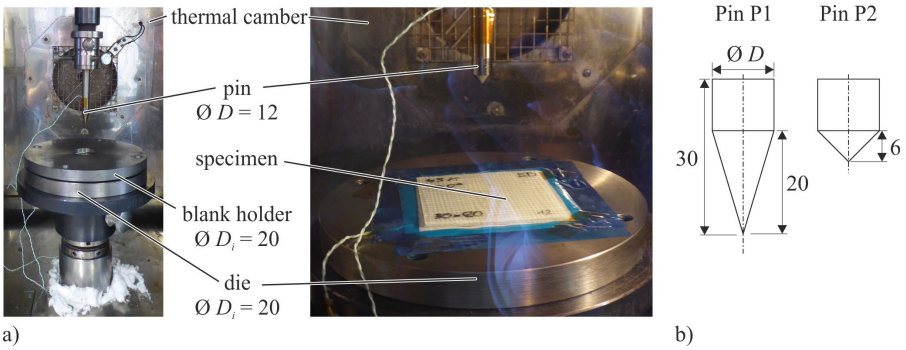

Fig. 1: a) Experimental setup for the pinning process and b) the two different pin geometries; all dimensions in mm.

Numerical setup

For the numerical simulations, the multi-filaments (MF) approach from [16] in combination with the ALE-method is used. The MF approach is based on a digital element chain [17], where the properties of the beam element summarize the properties of a certain amount of single fibres [18]. The setup is presented in Fig. 2 and the mesh information with the characteristic element length l_e are given in Table 1.

Due to the orthogonal four layers of MF, a half model is set up. The boundary conditions (BC) at the ends of all MF are defined to only allow a translation in fibre direction. Whereas, the nodes of the MF in the 90°-layers, which lie in the symmetry plane, can only move in-plane without rotational degrees of freedom. For both MF directions side walls with a penalty contact definition are implemented to avoid fibre movement out of the fluid domain. In accordance to the specimen dimension and the joining zone area, in 0°-direction the full length of 80 mm is modelled. For the 90°-layers, only 40 mm width of the layers is considered (Fig. 2 right). The tools and side walls are assumed to be rigid. Furthermore, except for the pin, they have fixed BC. Consequently, the clamping pressure between blank holder and die is not taken into account. Penalty contact definitions between MF, die and blank holder are defined. The pin has a displacement controlled translation definition in thickness direction through the layers. It is defined as a solid to avoid leakage in the ALE calculation. However, a special forming contact based on shell elements proved to be suited to model the sliding between MF and the pin. In order to apply this contact, a shell mesh is defined at the surface nodes of the solid. A constrained-based coupling algorithm between fluid and MF is defined. The beam element chain with a diameter of 0.5 mm representing the MF exhibits an elastic material behaviour with a Young's modulus of 57 MPa. For the matrix properties, a simplified viscous material model with a constant dynamic viscosity η of 530 Pas (based on experimental results) is used. The simulations are carried out with a mass scaling factor of 10,000.

Table 1: Mesh information of the numerical setup for pin P1.

Domain	l_e [mm]	Number of elements
Fluid	0.5	361,000
Multi-filament	1.5	4,988
Tools	-	54,904
Punch shell	-	8,204
Walls	-	21,120
Σ		450,816 elements; 480,678 nodes

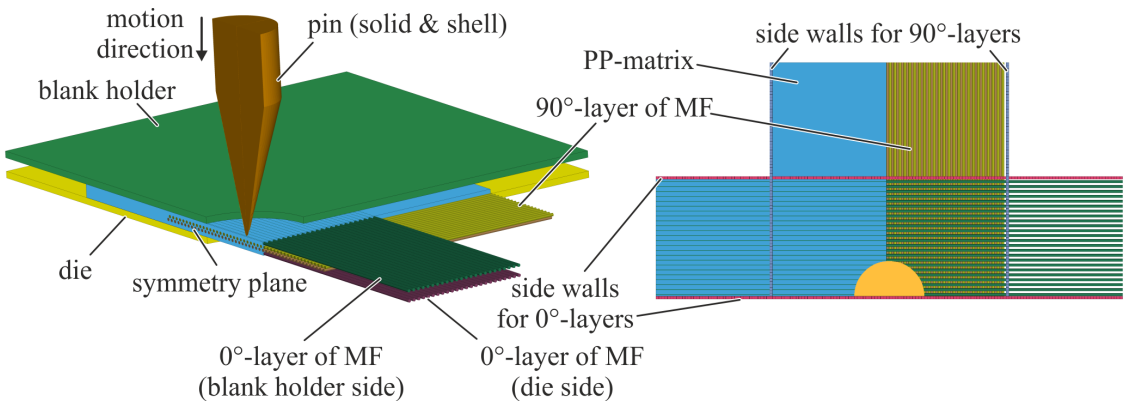

Fig. 2: Numerical setup for pinning process simulation with the pin P1.

Results and Validation

In Fig 3, the force-displacement curves of experiments where both pin geometries are investigated at two specimens (specimen number in brackets) are given. It can be seen that both the force peak and the descent of the curves of the blunt pin P2 are much higher than for the sharp pin P1. It is also evident that the force peak of P1 is achieved at higher displacements due to the long taper shape.

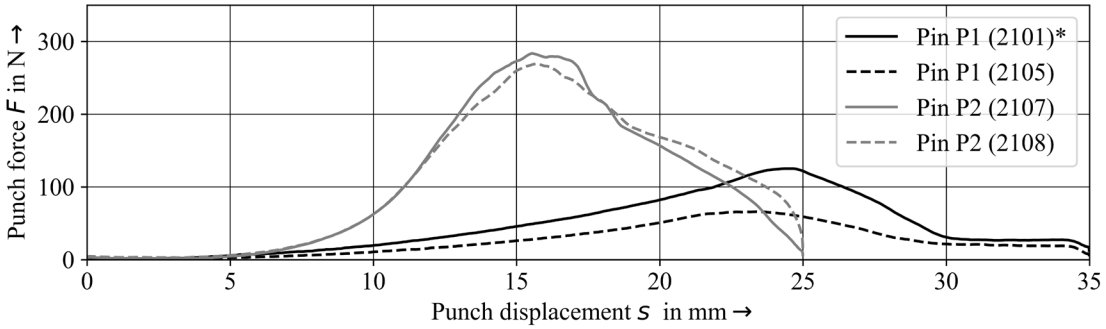

*Fig. 3: Force-displacement curves for the different pin geometries.*modified curve.*

The resultant material structure of the specimen ‘2105’ is presented in Fig. 4. On the blank holder side, a bulk is formed in 0°-direction consisting of matrix and in 90°-direction of yarns and matrix (1) (Fig. 4a). The 0°-yarns, pointing directly to the pin, are bent in piercing direction (2). The nearby yarns are displaced in 90°-direction (3). This radial reorientation leads to a torsion of fibre bundles in the yarn and the bulk forming on the free surface on the blank holder side (3) (Fig. 3a-b). The 90°-yarns are also bent in thickness direction (4). The increasing pin movement leads to a compaction, shifting and twisting (torsion) of all yarns in each layer (5) (Fig. 4b). Especially, the yarns of the die-sided layers are shifted out-of-plane. Here, on the one hand, the yarns distant to the pin are more shifted than twisted (6). On the other hand, the yarns close to the pin are splayed which is caused by the tool-yarn-friction and the motion of the pin (7). The friction also causes yarn shifting in fibre direction of 0°-yarns. The interaction between the different layers (e.g. FFI) lead to a shifting and bending (ondulation) of the 90°-yarns in radial direction to the pin (8) (Fig. 4c). The tool-yarn-friction, FFI and the yarn tension, result in a compaction of the yarns around the pin (5). Hence, matrix flow in the outer area of the piercing zone occurs, leading to matrix rich zones (9). Because of the shifting, bending and splaying, voids occur around the forming zone (10).

Likewise, the resultant material structure of specimen ‘2107’ in combination with pin P2 is investigated (Fig. 5). In contrast to pin P1, the bulk consists of matrix in both fibre directions (1) (Fig. 5a). As with pin P1, the yarns in all layers pointing directly to the pin are bent in thickness

direction (2, 4). Due to the blunt shape of pin P2, no reorientation in 90°-direction or bulk forming consisting of matrix and yarns on the blank holder side occur. Instead, all fibres are compacted, distorted and shifted in out-of-plane direction (5) (Fig. 5b). Therefore, the height *s* with 12.35 mm of the displaced splayed fibres (7) is higher in comparison the configuration of P1 with 3.86 mm. Due to the high displacement of the 0°-yarn and the FFI, the ondulation of the 90°-yarns increases (8) (Fig. 5c). In contrast to the P1 configuration, all yarns of each layer are twisted and distorted similarly in the piercing direction (5). The compaction in the resultant material structure is less than in P1, which reduces the formation of matrix rich zones (9). Because of the more significant reorientation phenomena of shifting, bending and torsion, more voids in the forming zone can be observed (10).

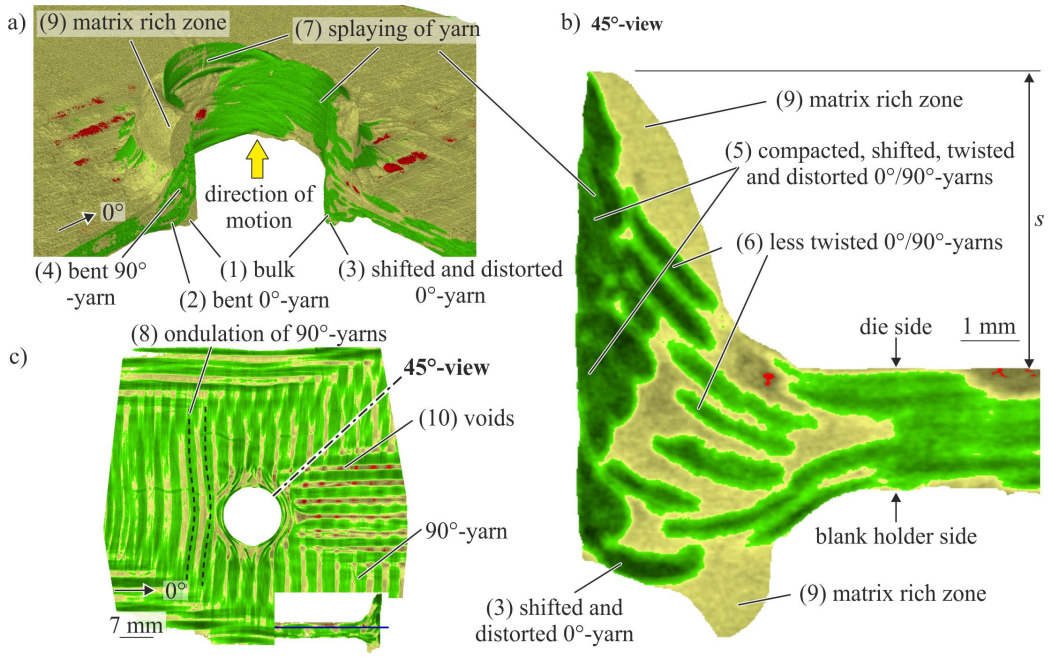

Fig. 4: CT-analysis of the resultant material structure for pin P1 (yarns highlighted in green, matrix in yellow and air volumes inside the TPC in red).

The results of the simulations for pin P1 with the resultant material structure are given in Fig. 6 and for P2 in Fig. 7. The modelling strategy is sensitive to the used pin geometry. Thus, the results show the influence of the pin sharpness on the resultant material structure. For pin P1, it can be seen that the MF of the blank holder sided layer are splayed (Fig. 6b). Also the bottom and mid layers are displaced continuously (Fig. 6b). Six MF next to the pin tip are excessively displaced and deformed, which can be caused by an unrealistic contact behaviour that results from the MF sticking to the pin and neglecting the clamping pressure (Fig. 6c). Excluding the “stuck” fibres, a displacement of approx. 7.4 mm is measured. Furthermore, the pin is not pushed through all layers despite a sufficient displacement (cf. Fig. 3).

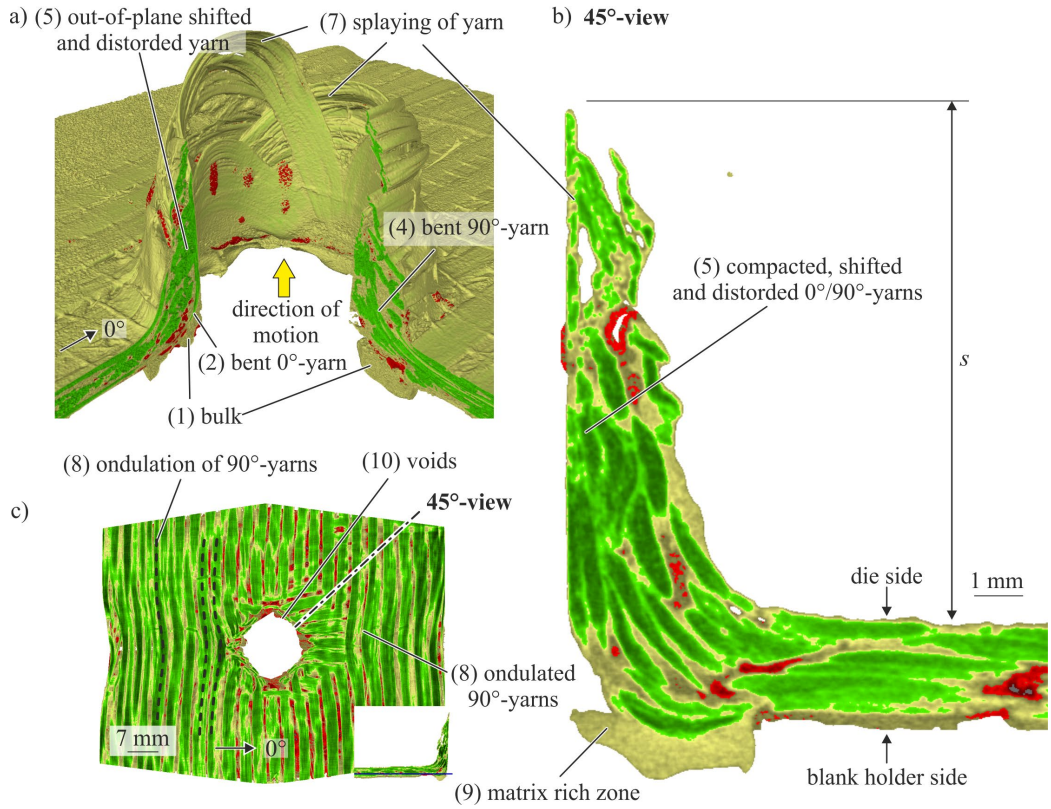

Fig. 5: CT-analysis of the resultant material structure for pin P2 (yarns highlighted in green, matrix in yellow and air volumes inside the TPC in red).

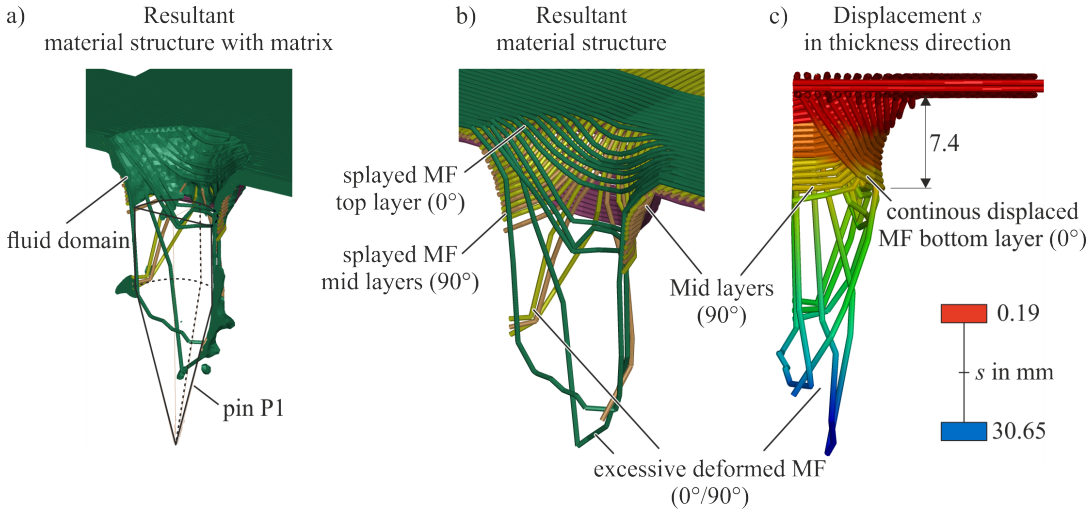

Fig. 6: Resultant material structure of pin P1 with the ALE method.

The resultant material structure for pin P2 shows a higher displacement of the MF in thickness direction in the piercing area. The splaying of the mid and bottom layer can be seen in (Fig. 7b and c). Additionally, an excessive deformation of the MF under the pin can be seen. It can be concluded that an unrealistic contact behaviour leads to the deformation. Due to the large displacement of the MF, the simulation exhibits areas with less matrix (Fig. 7a). Despite the non-accurate contact definition and the simplified material behaviour (constant viscosity, linear elastic), the results show main phenomena of the piercing process, which also occur in the experiment.

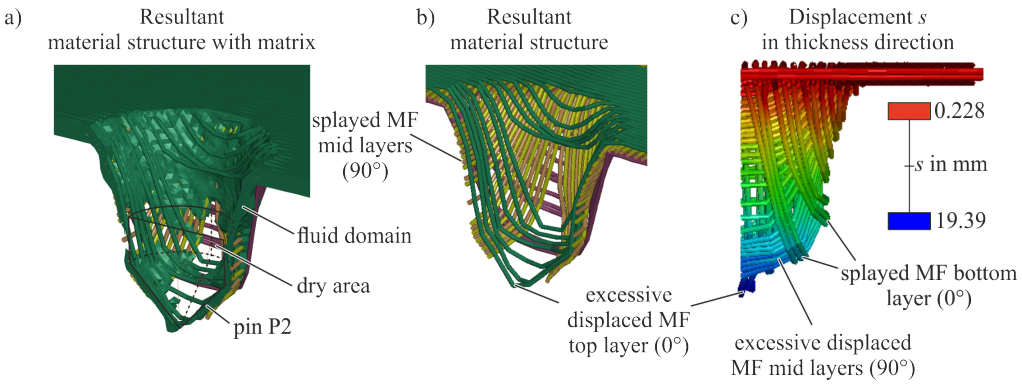

Fig. 7: Resultant material structure of pin P2 with the ALE method.

Summary and Outlook

The piercing forces and the resultant material structure of a piercing process are investigated with different pin shapes using isothermal process conditions. Based on the test setup, numerical simulations are carried out with the MF approach and ALE method. The numerical results represent the main phenomena of bending and displacement of MF in out-of-plane direction. Due to the limited contact definitions and the simplified assumptions used to determine the resultant stiffness of the MF, the shifting in fibre direction cannot be predicted accurately. For a more elaborated comparison, experimental and numerical investigations have to be carried out with focus on bending stiffness of yarns under process conditions. Additionally, the initial inhomogeneous textile architecture of the TPC sheets has to be modelled more accurately.

Funding

This research was funded by the Deutsche Forschungsgemeinschaft (DFG, German Research Foundation) -TRR 285-Project-ID 418701707 sub-project A03 and C04.

Acknowledgement

The authors are grateful to the Center for Information Services and High Performance Computing [Zentrum für Informationsdienste und Hochleistungsrechnen (ZIH)] at TU Dresden for providing its facilities for high throughput calculations.

References

[1] A. Galińska, C. Galiński. Mechanical Joining of Fibre Reinforced Polymer Composites to Metals-A Review. Part II: Riveting, Clinching, Non-Adhesive Form-Locked Joints, Pin and Loop Joining. Polymers (Basel) 2020;12(8). https://doi.org/10.3390/polym12081681

[2] F. Lambiase, S.I.Scipioni, C.-J. Lee, D.-C. Ko, Liu F. A State-of-the-Art Review on Advanced Joining Processes for Metal-Composite and Metal-Polymer Hybrid Structures. Materials (Basel) 2021;14(8). https://doi.org/10.3390/ma14081890

[3] B. Gröger, J. Troschitz, J. Vorderbrüggen, C. Vogel, R. Kupfer, G. Meschut et al. Clinching of Thermoplastic Composites and Metals-A Comparison of Three Novel Joining Technologies. Materials (Basel) 2021;14(9). https://doi.org/10.3390/ma14092286

[4] J. Troschitz, R. Füßel, R. Kupfer, M. Gude. Damage Analysis of Thermoplastic Composites with Embedded Metal Inserts Using In Situ Computed Tomography. J. Compos. Sci. 2022;6(10):287. https://doi.org/10.3390/jcs6100287

[5] H. Seidlitz, C. Gerstenberger, T. Osiecki, S. Simon, L. Kroll. High-performance lightweight structures with Fiber Reinforced Thermoplastics and Structured Metal Thin Sheets. JMSR 2014;4(1). https://doi.org/10.5539/jmsr.v4n1p28

[6] F. Hirsch, S. Müller, M. Machens, R. Staschko, N. Fuchs, M. Kästner. Simulation of self-piercing rivetting processes in fibre reinforced polymers: Material modelling and parameter identification. Journal of Materials Processing Technology 2017; 241(1):164–77. https://doi.org/10.1016/j.jmatprotec.2016.10.010

[7] J. Troschitz, B. Gröger, V. Würfel, R. Kupfer, M. Gude. Joining Processes for Fibre-Reinforced Thermoplastics: Phenomena and Characterisation. Materials (Basel) 2022;15(15). https://doi.org/10.3390/ma15155454

[8] N.W.A. Brown, C.M. Worrall, S.L. Ogin, P.A. Smith. Investigation into the mechanical properties of thermoplastic composites containing holes machined by a thermally-assisted piercing (TAP) process. Advanced Manufacturing: Polymer & Composites Science 2015;1(4):199–209. https://doi.org/10.1080/20550340.2015.1117748

[9] J. Popp, T. Kleffel, D. Römisch, T. Papke, M. Merklein, D. Drummer. Fiber Orientation Mechanism of Continuous Fiber Reinforced Thermoplastics Hybrid Parts Joined with Metallic Pins. Appl Compos Mater 2021;28(4):951–72. https://doi.org/10.1007/s10443-021-09892-0.

[10] M. Kraus, P. Frey, T. Kleffel, D. Drummer, M. Merklein. Mechanical joining without auxiliary element by cold formed pins for multi-material-systems. In: Proceedings of the 22nd international Esaform conference on material forming: Esaform 2019. AIP Publishing; 2019, p. 50006.

[11] S.T. Amancio-Filho, L.-A. Blaga (eds.). Joining of Polymer-Metal Hybrid Structures. Hoboken, NJ: John Wiley & Sons, Inc; 2018.

[12] E.E. Feistauer, S.T. Amancio-Filho. Ultrasonic Joining of Lightweight Alloy/Fiber-Reinforced Polymer Hybrid Structures. In: Amancio-Filho ST, Blaga L-A, editors. Joining of Polymer-Metal Hybrid Structures. Hoboken, NJ: John Wiley & Sons, Inc; 2018, p. 307–333.

[13] B. Gröger, A. Hornig, A. Hoog, M. Gude. Modelling of thermally supported clinching of fibre-reinforced thermoplastics: Approaches on mesoscale considering large deformations and fibre failure. ESAFORM 2021. https://doi.org/10.25518/esaform21.4293

[14] S. Roth, F. Pracisnore, S. Coutandin, J. Fleischer. A new approach for modelling the fibre path in bolted joints of continuous fibre reinforced composites. Composite Structures 2020;243(2):112184. https://doi.org/10.1016/j.compstruct.2020.112184

[15] J. Donea, A. Huerta, J.-P. Ponthot, Rodriguez-Ferran A. Arbitrary Lagrangian-Eulerian Methods. In: Stein E, Borst René de, Hughes TJR, editors. Encyclopedia of Computational Mechanics. Chichester, UK: John Wiley & Sons, Ltd; 2004, p. 657.

[16] S.D. Green, A.C. Long, B.S.F. El Said, S.R. Hallett. Numerical modelling of 3D woven preform deformations. Com. Struct. 2014; 108:747–56. https://doi.org/10.1016/j.compstruct.2013.10.015.

[17] Y. Wang, X. Sun. Digital-element simulation of textile processes. Composites Science and Technology 2001;61(2):311–9. https://doi.org/10.1016/S0266-3538(00)00223-2

[18] B. Gröger, V. Würfel, A. Hornig, M. Gude. Forming process induced material structure of fibre-reinforced thermoplastics - Experimental and numerical investigation of a bladder-assisted moulding process. Journal of Advanced Joining Processes 2022;5(7):100100. https://doi.org/10.1016/j.jajp.2022.100100